Iterative Data-Driven $\mathcal{H}_\infty$ Norm Estimation of Multivariable Systems With Application to Robust Active Vibration Isolation

Tom Oomen, *Member, IEEE*, Rick van der Maas, *Member, IEEE*, Cristian R. Rojas, *Member, IEEE*, and Håkan Hjalmarsson, *Fellow, IEEE*

***Abstract*— This paper aims to develop a new data-driven $\mathcal{H}_\infty$ norm estimation algorithm for model-error modeling of multivariable systems. An iterative approach is presented that requires significantly a fewer prior assumptions on the true system, hence it provides stronger guarantees in a robust control design. The iterative estimation algorithm is embedded in a robust control design framework with a judiciously selected uncertainty structure to facilitate high control performance. The approach is experimentally implemented on an industrial active vibration isolation system.**

***Index Terms*— Active vibration isolation system, data-driven control, data-driven modeling, model-free control, multivariable control, robust control, system identification for control, uncertain systems, uncertainty estimation.**

I. Introduction

ROBUSTNESS is of key importance in any feedback controlled system. An important example of such a feedback controlled system is an active vibration isolation system (AVIS) [1], [2], which is used to isolate highly accurate motion systems from external disturbances in multiple degree-of-freedom. The underlying idea of vibration isolation is based on the concept of skyhook damping, see [3]. Model-based control designs based on $\mathcal{H}_\infty$-optimization are considered in [4] and [5]. In [4], model uncertainty is explicitly considered. However, the uncertainty is based on inaccurate prior assumptions, leading to potentially conservative results.

Robustness analysis and robust control design hinge on an accurate quantification of model quality. On the one hand, several model-error modeling techniques have been developed that are based on the existing system identification methods [6]. For instance, in [7], the model error is quantified through the evaluation of the bias and variance errors of an estimated parametric model of the model residual. Such an approach often requires user intervention in the model parameterization step and relies on assumptions that are typically asymptotic in the data length. Alternatively, model-error modeling techniques have been proposed in [8] and [9] that are based on nonparametric frequency domain models. In [9], it is acknowledged that the use of a discrete frequency grid, which is unavoidable in any finite time experiment, leads to intergrid errors. In [8], these errors are ignored by the assumption that the frequency grid is sufficiently dense. In [9], these intergrid errors are bounded using prior assumptions, see also [10] for related approaches. However, bounding these errors generally leads to overly large estimates of the model error, as is also argued in [11, Sec. 9.5.2]. Finally, model validation techniques have been proposed, see [12] and [10] for frequency domain results and [13] for time domain results. However, such approaches often lead to overly optimistic estimates of the model errors unless appropriate validation experiments are designed [14].

On the other hand, recently in [15, Sec. 12.2], a data-driven iterative procedure is proposed that direct estimates the $\mathcal{H}_\infty$ norm of single-input single-output (SISO) systems. This enables its use in model-error modeling, since reliable robust control design methodologies are available that consider model errors as $\mathcal{H}_\infty$ norm bounded perturbations. In [16], the data-driven iterative $\mathcal{H}_\infty$ norm estimation is further extended, followed by a thorough stochastic analysis in [17]. In [18], the procedure is successfully applied for robust stability analysis of a SISO experimental setup.

Although the iterative data-driven $\mathcal{H}_\infty$ norm estimation algorithm has been thoroughly analyzed and successfully used for robustness stability analysis, it is not directly applicable to model-error modeling for achieving robust performance of general multivariable systems. First, the algorithms in [15, Sec. 12.2]–[17] are only suitable for SISO systems. Second, besides the size of the uncertainty in terms of the $\mathcal{H}_\infty$ norm, the uncertain model set highly depends on the model uncertainty structure and frequency weighting functions. Indeed, typical model-error modeling procedures involve the selection of a frequency-dependent weighting function to

Manuscript received February 18, 2013; revised July 10, 2013; accepted December 31, 2013. Manuscript received in final form January 24, 2014. Date of publication February 14, 2014; date of current version October 15, 2014. This work was supported in part by the European Research Council through the advanced Grant LEARN under Contract 267381, in part by the Swedish Research Council under Contract 621-2009-4017 and Contract 621-2011-5890, and in part by the Innovational Research Incentives Scheme under the VENI grant Precision Motion: Beyond the Nanometer under Grant 13073 awarded by The Netherlands Organisation for Scientific Research and Dutch Science Foundation. Recommended by Associate Editor T. Parisini.

T. Oomen and R. van der Maas are with the Eindhoven University of Technology, Department of Mechanical Engineering, Control Systems Technology Group, Eindhoven 5600 MB, The Netherlands (e-mail: t.a.e.oomen@tue.nl; r.j.r.v.d.maas@tue.nl).

C. R. Rojas and H. Hjalmarsson are with the Automatic Control Laboratory and Access Linnaeus Center, Electrical Engineering, KTH-Royal Institute of Technology, Stockholm S-100 44, Sweden (e-mail: cristian.rojas@ee.kth.se; hakan.hjalmarsson@ee.kth.se).

Color versions of one or more of the figures in this paper are available online at http://ieeexplore.ieee.org.

Digital Object Identifier 10.1109/TCST.2014.2303047

1063-6536 © 2014 IEEE. Personal use is permitted, but republication/redistribution requires IEEE permission.
See http://www.ieee.org/publications_standards/publications/rights/index.html for more information.

Authorized licensed use limited to: Zhejiang University. Downloaded on November 15,2024 at 14:52:51 UTC from IEEE Xplore. Restrictions apply.

shape the uncertainty, see [19, Sec. 7.4.3] for details in this direction. However, iterative data-driven $\mathcal{H}_\infty$ norm estimation algorithms do not provide the required frequency-dependent shape of the model error and cannot be used as a basis for designing frequency-dependent weighting functions. Indeed, in [18], the algorithms are only used as an *a posteriori* stability verification. This paper aims to develop a data-driven iterative $\mathcal{H}_\infty$ norm estimation procedure for model-error modeling of multivariable systems for robust control.

The contributions of this paper are threefold.

1) A novel multivariable data-driven $\mathcal{H}_\infty$ norm estimation procedure is presented that applies to general multi-input, multi-output (MIMO) systems. In addition to iteratively determining the worst case frequency, as in [15, Sec. 12.2]–[17], the proposed algorithm in this paper is also able to determine the worst case input and output direction.
2) The proposed multivariable data-driven $\mathcal{H}_\infty$ norm estimation procedure is used in conjunction with a new model uncertainty structure that has recently been developed in [20]. This new model uncertainty structure renders the use of weighting functions superfluous in model-error modeling by directly connecting the size of model uncertainty and the control criterion. This enables the use of the proposed data-driven $\mathcal{H}_\infty$ norm estimation procedure for model-error modeling of multivariable systems for high performance robust control.
3) Application of the procedure to a multivariable industrial AVIS system, which as follows:
   a) confirms that the multivariable data-driven $\mathcal{H}_\infty$ norm estimation procedure converges and performs reliably when implemented on an industrial system;
   b) reveals higher accuracy of the estimated model error compared with an alternative model-error modeling procedure;
   c) confirms that the resulting model set leads to enhanced vibration isolation.

Preliminary research results related to C1 appear as [21], this paper extends this with an extensive theoretical and experimental results. In addition, this paper contains the new Contributions C2 and C3.

The main results of this paper are presented in the noise-free situation to facilitate the exposition. An analysis of the situation of additive stochastic noise is presented in Section III-C3.

This paper is organized as follows. In Section II, the AVIS and the control goal are presented. Then, in Section III, the multivariable data-driven $\mathcal{H}_\infty$ norm estimation procedure is presented, leading to Contribution C1. Then, in Section IV, the proposed $\mathcal{H}_\infty$ norm estimation procedure is used in conjunction with the new model uncertainty structure in [20], constituting Contribution C2. In Section V, experimental results of the proposed uncertainty modeling procedure are presented. The resulting model set is then used in Section VI to design and implement a robust controller on the AVIS system. Hence, Sections V and VI contain Contribution C3. Finally, a discussion and a conclusion are presented in Section VII.

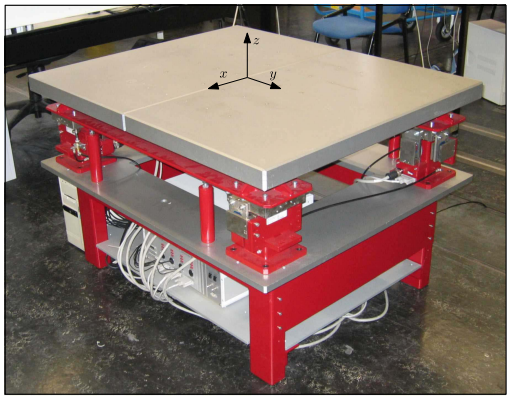

Fig. 1. Photograph of the experimental AVIS setup. The rotation around the x-axis is denoted by ϕ.

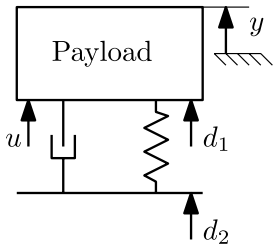

Fig. 2. Schematic illustration of the AVIS.

II. Description of AVIS and Control Goal

A. Active Vibration Isolation System

The AVIS in Fig. 1 is considered in this paper. The system consists of two main parts, i.e., a movable payload and a chassis that is connected to the floor. The payload and chassis are connected by four isolator modules. On the one hand, these isolator modules provide passive damping through a pneumatic airmount. On the other hand, the isolator modules are equipped with Lorentz motors and geophones that enable active vibration isolation. Specifically, the isolation modules are each equipped with two motors, leading to eight actuators in total. The currents applied to the motors are denoted $a = [a_1 \;\; a_2 \;\; a_3 \;\; a_4 \;\; a_5 \;\; a_6 \;\; a_7 \;\; a_8.]$. In addition, three out of four modules are equipped with two geophones each that construct measurements of the velocity, leading to six sensors, which are denoted $s = [s_1 \;\; s_2 \;\; s_3 \;\; s_4 \;\; s_5 \;\; s_6.]$. The inputs and outputs of the system are rigid-body decoupled with respect to the Cartesian coordinate frame shown in Fig. 1. The manipulated input and output are denoted

$$u = T_u a \tag{1}$$

$$y = T_y s \tag{2}$$

respectively, where $T_u \in \mathbb{R}^{6\times 8}$ and $T_y \in \mathbb{R}^{6\times 6}$. Finally, the true system P_o is given by $P_o : u \mapsto y$.

The goal of the AVIS is to isolate the payload with respect to exogenous disturbances. The AVIS is schematically shown in Fig. 2. The signal d_1 refers to force disturbances that directly affect the payload, and d_2 refers to force disturbances that are induced by floor vibrations. The goal is to keep the absolute velocity of the payload equal to zero by manipulating the

Authorized licensed use limited to: Zhejiang University. Downloaded on November 15,2024 at 14:52:51 UTC from IEEE Xplore. Restrictions apply.

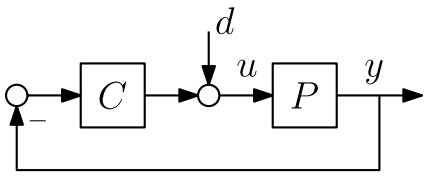

Fig. 3. Simplified feedback interconnection for vibration isolation.

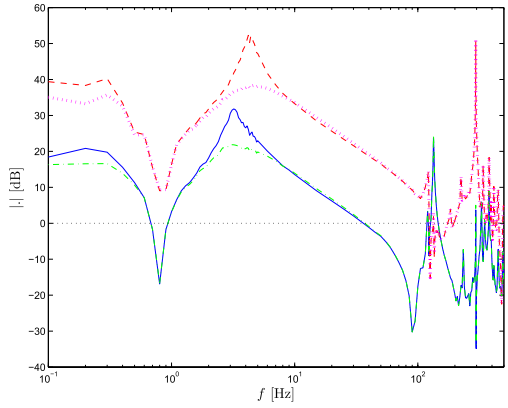

Fig. 4. Active vibration isolation through skyhook damping: identified frequency response of open-loop P_o in z- (solid blue line) and ϕ-direction (dashed red line) and identified frequency response of closed-loop $P_o^{\mathrm{cl,exp}}$ in z- (dashed-dotted green line) and ϕ-direction (dotted magenta line).

input u through the velocity measurement y, see (2). The key advantage of active vibration control compared with the passive isolation by the pneumatic airmounts is the availability of absolute velocity measurements. This enables skyhook damping [3], which connects the fictive damper (implemented as a control algorithm) to the fixed world. Thus, skyhook damping implies that y should be kept as small as possible for both disturbances d_1 and d_2. This is in sharp contrast to the situation where velocity measurements relative to the floor are available, in which case y should be kept as small as possible only if $d_2 = 0$.

The resulting feedback interconnection is shown in Fig. 3, where

$$d = d_1 + H_d d_2$$

and H_d is a causal stable transfer function matrix that characterizes the transfer of the floor vibrations through the pneumatic airmount to the payload.

To show the potential performance improvement by skyhook damping, an initial controller C^{exp} is designed. This controller consists of a multiloop SISO controller, where each diagonal element is a gain with high-frequency roll-off, see Fig. 14 in Section VI-A for the diagonal elements corresponding to the z- and ϕ-direction. The resulting closed-loop transfer function

$$P_o^{\mathrm{cl,exp}} : d \mapsto y = P_o(I + C^{\mathrm{exp}} P_o) \tag{3}$$

characterizes the closed-loop disturbance attenuation properties. In Fig. 4, frequency response function measurements of the open-loop system P_o and the closed-loop system $P_o^{\mathrm{cl,exp}}$ are depicted in the vertical translational direction z. The actual identification of these frequency response functions is described in Section V. Clearly, Fig. 4, reveals that the controller C^{exp} damps the resonance phenomenon at approximately 3.2 Hz by 10 dB in the translational z-direction.

Although C^{exp} increases the damping properties of the AVIS, see Fig. 4, the increased damping is insufficient for satisfactory control performance. This will be confirmed by the experimental results in Section VI-B, specifically Figs. 16 and 17. Analysis of the power spectral densities in Fig. 17 reveals a dominant frequency content between 1 and 10 Hz.

B. Control Goal and Approach

The goal in this paper is to improve vibration isolation properties of the AVIS through enhanced controller design. The key performance limiting factor in increasing the gain of the controller C^{exp}, and hence increasing the skyhook damping, involves the high-frequency flexible dynamics beyond 100 Hz, as can be observed in Fig. 4. Thus, performance and robustness objectives have to be appropriately specified. The pursued approach to achieve high performance active vibration isolation is a multivariable robust controller design.

The performance objectives are specified using a criterion $\mathcal{J}(P, C)$, where the goal is to compute the optimal controller

$$C^{\mathrm{opt}} = \arg\min \mathcal{J}(P_o, C).$$

Before specifying $\mathcal{J}(P, C)$ in more detail, see Section II-C, the connection between the control objective and the true unknown system P_o is established in further detail.

To address robustness objectives, note that the minimization of $\mathcal{J}(P_o, C)$ requires knowledge of P_o. This knowledge is reflected by a model set $\mathcal{P}$. This model set $\mathcal{P}$ will be defined more precisely in Section II-D. The key property of this model set $\mathcal{P}$ is that it will be chosen such that it encompasses the true AVIS dynamical behavior, i.e., including the high-frequency flexible dynamics. Hence, the assumption

$$P_o \in \mathcal{P} \tag{4}$$

is assumed to hold throughout this paper. The key motivation for considering a model set is the fact that any model is uncertain and cannot represent the true system behavior exactly. In view of (4), given the model set $\mathcal{P}$, the robust controller synthesis

$$C^{\mathrm{RP}} = \arg\min_C \mathcal{J}_{\mathrm{WC}}(\mathcal{P}, C) \tag{5}$$

is considered, where $\mathcal{J}_{\mathrm{WC}}(\mathcal{P}, C) = \sup_{P\in\mathcal{P}} \mathcal{J}(P, C)$. This provides a performance guarantee when implementing C^{RP} on the true system, since by (4), the bound

$$\mathcal{J}(P_o, C^{\mathrm{RP}}) \leq \mathcal{J}_{\mathrm{WC}}(\mathcal{P}, C^{\mathrm{RP}}) \tag{6}$$

holds.

To facilitate the exposition, a two-input two-output robust feedback controller is designed for the z- and ϕ-direction

$$\begin{bmatrix} u_z \\ u_\phi \end{bmatrix} = C^{\mathrm{RP}} \begin{bmatrix} y_z \\ y_\phi \end{bmatrix}.$$

The presented approach applies equally well to the full multivariable situation, i.e., three rotations and three translations.

Authorized licensed use limited to: Zhejiang University. Downloaded on November 15,2024 at 14:52:51 UTC from IEEE Xplore. Restrictions apply.

In this paper, the selection of a rotational and translational degree-of-freedom is made to show that the presented approach automatically scales the uncertainty channels, see (28). Hence, it automatically deals with various units of the measurements. Note that, all the physical actuators a and sensors s are typically used due to T_u and T_y in (1) and (2), respectively.

C. Control Criterion

The control goal in this paper is specified by

$$\mathcal{J} = \|WT(P, C)V\|_\infty \tag{7}$$

where

$$T(P, C) = \left[\begin{array}{c|c} T_{11} & T_{12} \\ \hline T_{21} & T_{22} \end{array}\right] = \begin{bmatrix} P \\ I \end{bmatrix} (I + \mathrm{CP})^{-1} \begin{bmatrix} C & I \end{bmatrix}. \tag{8}$$

The transfer function matrix $T(P, C)$ maps

$$\begin{bmatrix} r_2 \\ r_1 \end{bmatrix}$$

onto

$$\begin{bmatrix} y \\ u \end{bmatrix}$$

where r_1 corresponds to d in Fig. 3 and r_2 is an additional signal, see Fig. 7 in Section IV-C for a block diagram. In addition, W and V in (7) are stable and minimum-phase weighting filters. The motivation for considering the $\mathcal{H}_\infty$ norm in (7) is to enable a systematic robust controller synthesis.

A four-block problem is considered, i.e., $T(P, C)$ in (8) contains four blocks. The four-block problem guarantees internal stability of the resulting optimal controller. This has important implications from a theoretical perspective, since it will enable the construction of a specific coprime factorization that leads to (28). In addition, the four-block problem enables the use of the systematic loop-shaping approach in [22] to select W and V such that it enhances active vibration isolation performance. Note that, the relevant closed-loop transfer function for vibration isolation is essentially given by (3). Interestingly, the loop-shaping approach in [22] is essentially based on the fact that the loop-gain CP is the only degree-of-freedom in shaping the four-block problem (8). In this paper, the transparent connection between shaping the loop-gain CP and the relevant transfer function (3) is exploited to design the weighting functions.

In the considered design framework, so-called loop-shaping weighting filters W_1 and W_2 are adopted that shape the desired open-loop gain $W_2\mathrm{P}W_1$. Next, observe that the initial controller leads to a certain loop-gain $C^{\mathrm{exp}}P$. The desired loop-gain typically has a smaller amplitude in the low frequency range compared with $W_2\mathrm{P}W_1$. Hence, the rationale in this paper to design the weighting filter W_1 and W_2 is to increase the gain of C^{exp}

$$W_1 = \begin{bmatrix} 1 & 0 \\ 0 & 1 \end{bmatrix}, \quad W_2 = \begin{bmatrix} 19.9 & 0 \\ 0 & 11.75 \end{bmatrix} C^{\mathrm{exp}}.$$

Although the design procedure to select W_2 resembles the controller C^{exp}, a robust controller synthesis procedure is required to deliver a robustly stabilizing feedback controller. These weighting functions W_2 and W_1 directly fit in criterion (7) through

$$W = \begin{bmatrix} W_2 & 0 \\ 0 & W_1^{-1} \end{bmatrix}, \quad V = \begin{bmatrix} W_2^{-1} & 0 \\ 0 & W_1 \end{bmatrix}.$$

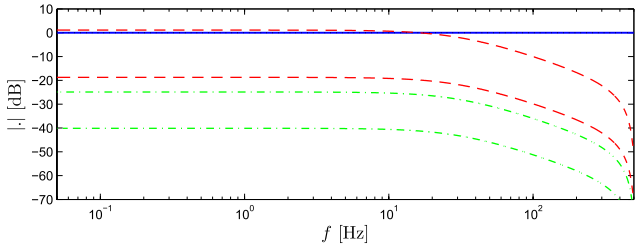

Fig. 5. Singular values of weighting filters W_1 (solid blue line), W_2 (dashed red line), and initial controller C^{exp} (dashed-dotted green line).

D. Identification of $\mathcal{P}$ Using $\mathcal{H}_\infty$ Norm Bounded Perturbations

The uncertain model set $\mathcal{P}$ that is introduced in Section II-B is constructed as an $\mathcal{H}_\infty$ norm bounded perturbation around a nominal model $\hat{P}$

$$\mathcal{P} = \{P | P = \mathcal{F}_u(\hat{H}(\hat{P}), \Delta_u), \Delta_u \in \mathbf{\Delta}_u\} \tag{9}$$

where $\hat{H}(\hat{P})$ represents the nominal model $\hat{P}$ and uncertainty structure. Also, the upper linear fractional transformation (LFT) is given by

$$\mathcal{F}_u(\hat{H}, \Delta_u) = \hat{H}_{22} + \hat{H}_{21}\Delta_u(I - \hat{H}_{11}\Delta_u)^{-1}\hat{H}_{12}.$$

As an example of (9), note that $\hat{H}(\hat{P})$ in the case of additive uncertainty $\hat{P} + \Delta_u$ is given by $H_{11} = 0$, $H_{12} = H_{21} = I$, and $H_{22} = \hat{P}$. In addition, unstructured model uncertainty is considered

$$\mathbf{\Delta}_u := \{\Delta_u | \|\Delta_u\|_\infty \leq \gamma\}. \tag{10}$$

To actually identify $\mathcal{P}$, three aspects are of importance:

1) identifying a nominal model $\hat{P}$;
2) constructing a model uncertainty structure, see $\hat{H}(\hat{P})$;
3) determining the size of model uncertainty γ in (10).

In the following section, a new approach for the latter aspect, i.e., determining γ, is presented. The former two aspects are subsequently addressed in Section IV, leading to a complete procedure that encompasses 1)–3).

III. Data-Driven Approach to Multivariable Uncertainty Modeling

In this section, a novel procedure is presented to estimate the size γ of Δ_u, given a nominal model $\hat{P}$ and uncertainty structure $\hat{H}(\hat{P})$. Therefore, γ depends on the choice of $\hat{P}$ and the uncertainty structure, where a suitable structure will be presented in Section IV. In addition, in view of (4), γ depends on the true system P_o. To show this, let Δ_o uniquely generate P_o in (9)

$$P_o = \mathcal{F}_u(\hat{H}(\hat{P}), \Delta_o). \tag{11}$$

Authorized licensed use limited to: Zhejiang University. Downloaded on November 15,2024 at 14:52:51 UTC from IEEE Xplore. Restrictions apply.

In this case

$$\gamma = \|\Delta_o\|_\infty$$

is the minimum-norm bound such that the model set defined by (9) and (10) satisfies (4). Thus, the goal in model-error modeling essentially is to determine the $\mathcal{H}_\infty$ norm of the model error Δ_o. Note that, Δ_o generally is a dynamic system, e.g., in the case of additive uncertainty, $\Delta_o = \hat{P} - P_o$.

The pursued approach to estimate γ is to perform experiments on Δ_o. To achieve this, the input u_Δ is applied to Δ_o and the output $y_\Delta = \Delta_o u_\Delta$ is measured. Note that, in general experimentation on Δ_o involves both an experiment on the true system P_o and a simulation with the model $\hat{P}$. For instance, in the case of additive uncertainty, $y_\Delta = \Delta_o u_\Delta = \hat{P}u_\Delta - P_o u_\Delta$.

The key idea in this paper is to directly estimate the size γ of Δ_o based on measured data, hence without the need for identification of an intermediate model. In contrast, the approach in [7] involves the estimation of an auxiliary model of the model error Δ_o, whereas [8] and [9] employ a nonparametric model, i.e., an identified frequency response function, of Δ_o. In these approaches, the identified model is subsequently used to compute the $\mathcal{H}_\infty$ norm.

Next, the basic procedure is presented, revealing that the auxiliary model estimation step can be rendered superfluous.

A. Iterative Data-Driven $\mathcal{H}_\infty$ Norm Estimation: SISO Systems

In this section, the basic principle for data-driven $\mathcal{H}_\infty$ norm estimation is presented. To introduce the mechanism, first assume that Δ is SISO and linear time invariant. Hence, $\Delta(z) = \sum_{k=0}^{\infty} \delta_k z^{-k}$, with δ_k, $k = 0, \ldots, \infty$ the Markov parameters of the system. Next, recall that the $\mathcal{H}_\infty$ norm is an induced norm i.e., $\|\Delta\|_\infty = \|\Delta\|_{i2}$ see [19, App. A.5.7] for a proof. Assume that the signals have finite length $N \in \mathbb{N}$, i.e., $\underline{u_\Delta}, \underline{y_\Delta} \in \mathbb{R}^{N\times 1}$, hence

$$\|\underline{\Delta}\|_{i2} = \sup_{\underline{u_\Delta} \in \mathbb{R}^{N\times 1}\setminus 0} \frac{\|\underline{y_\Delta}\|_2}{\|\underline{u_\Delta}\|_2}. \tag{12}$$

Note that, $\|\underline{\Delta}\|_{i2} \to \|\Delta\|_\infty$ for $N \to \infty$, see [17, Th. 3] for a proof. Next, on the finite time interval of length N

$$\underline{y_\Delta} = \underline{\Delta}\,\underline{u_\Delta} \tag{13}$$

where no measurement noise is assumed and

$$\underline{\Delta} = \begin{bmatrix} \delta_0 & 0 & 0 & \ldots & 0 \\ \delta_1 & \delta_0 & 0 & & 0 \\ \vdots & \vdots & & \ddots & 0 \\ \delta_{N-1} & \delta_{N-2} & \delta_{N-3} & \ldots & \delta_0 \end{bmatrix}.$$

Thus, (12) is equivalent to

$$\|\underline{\Delta}\|_{i2} = \sup_{\underline{u_\Delta} \in \mathbb{R}^{N\times 1}\setminus 0} \sqrt{\frac{\underline{u_\Delta}^T \underline{\Delta}^T \underline{\Delta}\,\underline{u_\Delta}}{\underline{u_\Delta}^T \underline{u_\Delta}}} = \sqrt{\lambda^{\max}(\underline{\Delta}^T \underline{\Delta})}. \tag{14}$$

Now, observe that

$$\underline{\Delta}^T = \mathcal{T}_N \underline{\Delta} \mathcal{T}_N \tag{15}$$

where

$$\mathcal{T}_N = \begin{bmatrix} 0 & \ldots & 0 & 1 \\ 0 & \ldots & 1 & 0 \\ \vdots & & & \vdots \\ 1 & \ldots & 0 & 0 \end{bmatrix}$$

i.e., $\mathcal{T}_N$ is an involutory permutation matrix of size $N \times N$. Here, $\mathcal{T}_N$ has the interpretation of a time-reversal operator. Next, (15) reveals that $\mathcal{T}_N \underline{\Delta}$ is symmetric, hence

$$\|\underline{\Delta}\|_{i2} = \lambda^{\max}(\mathcal{T}_N \underline{\Delta}). \tag{16}$$

Thus, $\|\underline{\Delta}\|_{i2}$ equals the largest eigenvalue of the matrix $\mathcal{T}_N \underline{\Delta}$. Hence, given the impulse response δ_i, $i = 1, \ldots, N$, $\|\underline{\Delta}\|_{i2}$ can directly be computed through an eigenvalue analysis. In contrast, in this paper, another approach is pursued to determine $\|\underline{\Delta}\|_{i2}$ that does not require knowledge of δ_i, $i = 1, \ldots, N$. Such an approach is given next.

Procedure 1 (SISO $\|\underline{\Delta}\|_{i2}$ Estimation): Perform the following sequence of steps.

1) Set $n = 1$ and initialize with arbitrary $\underline{u_\Delta}^{(1)} \in \mathbb{R}^{N\times 1}\setminus 0$.
2) Determine $\underline{y_\Delta}^{(n)} = \underline{\Delta}\,\underline{u_\Delta}^{(n)}$ by performing an experiment on the system.
3) Time-reverse: $\underline{x_\Delta}^{(n)} = \mathcal{T}_N \underline{y_\Delta}^{(n)}$.
4) Set $\underline{u_\Delta}^{(n+1)} = \underline{x_\Delta}^{(n)}$.
5) Set $n \mapsto n+1$ and repeat from Step 2 until a stopping criterion is met.

Procedure 1 coincides with the power method [23, Sec. 7.3.1], which is an iterative algorithm to determine the maximal eigenvalue of a matrix. It is well known that this estimator

$$\hat{\gamma}_1^{(n)} = \frac{\left(\underline{u_\Delta}^{(n)}\right)^T \underline{x_\Delta}^{(n)}}{\left(\underline{u_\Delta}^{(n)}\right)^T \underline{u_\Delta}^{(n)}} \tag{17}$$

converges under mild conditions to $\|\underline{\Delta}\|_{i2}$ for $n \to \infty$.

Essentially, two approaches can be pursued to complete Step 2 in Procedure 1. On the one hand, $\underline{\Delta}^{(n)}\underline{u_\Delta}^{(n)}$ can be evaluated on a model using impulse response coefficients δ_i, $i = 1, \ldots, N$. On the other hand, the approach taken in this paper is to perform an experiment of length N on the true system Δ_o to evaluate $\underline{\Delta}^{(n)}\underline{u_\Delta}^{(n)}$. Thus, Procedure 1 does not need any structural knowledge of Δ_o.

Summarizing, the iterative procedure 1 leads to an estimate $\hat{\gamma}_1^{(n)}$ of $\|\Delta_o\|_\infty$ for a sufficiently large number of iterations n and sufficiently long experiment length N. Each iteration requires one experiment of length N on the true system Δ_o, provided that Δ_o is SISO. Since the approach is data-driven, the only computational step involves (17), which has linear complexity in N and thus is not restrictive for large N.

In the following section, $\mathcal{H}_\infty$ norm estimation of MIMO systems is investigated.

B. Data-Driven $\mathcal{H}_\infty$ Norm Estimation of MIMO Systems

In this section, a novel procedure for estimating the $\mathcal{H}_\infty$ norm of MIMO systems is presented. It turns out that Procedure 1 does not directly apply to MIMO systems, since (15) is not valid for general MIMO systems. Hence, MIMO systems introduce a significant complication when compared with the SISO case in Section III-A.

Authorized licensed use limited to: Zhejiang University. Downloaded on November 15,2024 at 14:52:51 UTC from IEEE Xplore. Restrictions apply.

To develop a data-driven $\mathcal{H}_\infty$ norm estimator for MIMO systems, consider the transfer function matrix of the MIMO system Δ with p outputs and q inputs

$$\Delta = \begin{bmatrix} \Delta_{11} & \dots & \Delta_{1q} \\ \vdots & \ddots & \vdots \\ \Delta_{p1} & \dots & \Delta_{pq} \end{bmatrix} \in \mathcal{RH}_\infty^{p\times q}$$

with finite time representation for experiment length N

$$\underbrace{\begin{bmatrix} \underline{y}_{\Delta 1} \\ \vdots \\ \underline{y}_{\Delta p} \end{bmatrix}}_{=:\underline{y}_\Delta} = \underbrace{\begin{bmatrix} \underline{\Delta}_{11} & \dots & \underline{\Delta}_{1q} \\ \vdots & \ddots & \vdots \\ \underline{\Delta}_{p1} & \dots & \underline{\Delta}_{pq} \end{bmatrix}}_{=:\underline{\Delta}} \underbrace{\begin{bmatrix} \underline{u}_{\Delta 1} \\ \vdots \\ \underline{u}_{\Delta q} \end{bmatrix}}_{=:\underline{u}_\Delta} \tag{18}$$

where $\underline{u}_{\Delta i} \in \mathbb{R}^{N\times 1}$, $i = 1, \dots, q$, and $\underline{y}_{\Delta i} \in \mathbb{R}^{N\times 1}$, $i = 1, \dots, p$. In addition, $\underline{\Delta} \in \mathbb{R}^{pN\times qN}$.

To proceed, observe that (14) is also valid for the multivariable system (18). Next, note that

$$\underline{\Delta}^T = \underbrace{\begin{bmatrix} \mathcal{T}_N & & 0 \\ & \ddots & \\ 0 & & \mathcal{T}_N \end{bmatrix}}_{=:\mathcal{T}_{qN}} \underbrace{\begin{bmatrix} \underline{\Delta}_{11} & \dots & \underline{\Delta}_{p1} \\ \vdots & \ddots & \vdots \\ \underline{\Delta}_{1q} & \dots & \underline{\Delta}_{pq} \end{bmatrix}}_{=:\underline{\widetilde{\Delta}}} \underbrace{\begin{bmatrix} \mathcal{T}_N & & 0 \\ & \ddots & \\ 0 & & \mathcal{T}_N \end{bmatrix}}_{=:\mathcal{T}_{pN}}$$

i.e., $\underline{\widetilde{\Delta}}$ is the finite time representation of the transfer function matrix

$$\widetilde{\Delta} = \begin{bmatrix} \Delta_{11} & \dots & \Delta_{p1} \\ \vdots & \ddots & \vdots \\ \Delta_{1q} & \dots & \Delta_{pq} \end{bmatrix}.$$

In general, $\widetilde{\Delta} \neq \Delta$. Thus, an analogous step from (14)–(16) can only be made in the restrictive case, where $\widetilde{\Delta} = \Delta$, i.e., if the system is symmetric. Thus, the case $\widetilde{\Delta} \neq \Delta$ requires a different approach. The key step in the forthcoming developments is the observation that

$$\widetilde{\Delta} = \sum_{i=1}^{q}\sum_{j=1}^{p} \mathcal{I}_{ij}\, \Delta\, \mathcal{I}_{ij} \tag{19}$$

where

$$\mathcal{I}_{ij} = \begin{bmatrix} 0 & \dots & 0 & \dots & 0 \\ \vdots & \ddots & & \ddots & 0 \\ 0 & \dots & 1 & \dots & 0 \\ \vdots & \ddots & & \ddots & \vdots \\ 0 & \dots & 0 & \dots & 0 \end{bmatrix} \in \mathbb{R}^{q\times p}$$

and the 1 is on the (i, j)th location. To derive the finite time equivalent of (19), note that the finite time representation of $\mathcal{I}_{ij}$ is given by

$$\underline{\mathcal{I}}_{ij} = \begin{bmatrix} 0 & \dots & 0 & \dots & 0 \\ \vdots & \ddots & & \ddots & 0 \\ 0 & \dots & I_N & \dots & 0 \\ \vdots & \ddots & & \ddots & \vdots \\ 0 & \dots & 0 & \dots & 0 \end{bmatrix} \in \mathbb{R}^{qN\times pN} \tag{20}$$

where $\underline{\mathcal{I}}_{ij}$ is a block-diagonal matrix of $q \times p$ blocks of dimension $N \times N$. Also, the (i, j)th block-element is equal to an identity matrix of size N. Note that the system $\mathcal{I}_{ij}$ can be interpreted as a static system, i.e., containing only a direct feedthrough term, leading to a diagonal matrix in (20). Next

$$\underline{\widetilde{\Delta}} = \sum_{i=1}^{q}\sum_{j=1}^{p} \underline{\mathcal{I}}_{ij}\, \underline{\Delta}\, \underline{\mathcal{I}}_{ij}. \tag{21}$$

The result (21) is the basis for the following procedure, which constitutes Contribution C1 of this paper.

Procedure 2 (MIMO $\|\underline{\Delta}\|_{i2}$ Estimation): Perform the following sequence of steps.

1) Set $n = 1$ and initialize with arbitrary $\underline{u}_\Delta{}^{(1)} \in \mathbb{R}^{qN\times 1}$, $\underline{u}_\Delta{}^{(1)} \neq 0$.
2) Determine $\underline{y}_\Delta{}^{(n)} = \underline{\Delta}\underline{u}_\Delta{}^{(n)}$ by performing an experiment on the system.
3) Time-reverse: $\underline{x}_\Delta{}^{(n)} = \mathcal{T}_{pN}\underline{y}_\Delta{}^{(n)}$.
4) Set $\underline{z}_\Delta{}^{(n)} = 0$ and perform pq experiments

```
for i = 1, …, q
    for j = 1, …, p
```

$$\underline{z}_\Delta{}^{(n)} \mapsto \underline{z}_\Delta{}^{(n)} + \underline{\mathcal{I}}_{ij}\underline{\Delta}\underline{\mathcal{I}}_{ij}\underline{x}_\Delta{}^{(n)}$$

```
    end
end.
```

5) Time reverse: $\underline{w}_\Delta{}^{(n)} = \mathcal{T}_{qN}\underline{z}_\Delta{}^{(n)}$.
6) Set $\underline{u}_\Delta{}^{(n+1)} = \underline{w}_\Delta{}^{(n)}$.
7) Set $n \mapsto n + 1$ and repeat from Step 2 until a stopping criterion is met.

The multivariable $\mathcal{H}_\infty$ norm can then be estimated as

$$\hat{\gamma}_2^{(n)} = \sqrt{\frac{\left(\underline{u}_\Delta{}^{(n)}\right)^T \underline{w}_\Delta{}^{(n)}}{\left(\underline{u}_\Delta{}^{(n)}\right)^T \underline{u}_\Delta{}^{(n)}}} \tag{22}$$

where in contrast to Procedure 1, a square root appears because the reduction from two experiments to a single experiment per step in the SISO procedure [based on (14)–(16)] is not made in the derivation of Procedure 2.

Basically, (19) and Procedure 2 recast the evaluation of $\underline{\Delta}^T$ as $p \cdot q$ experiments on $\underline{\Delta}$, for which the true system Δ_o is available for evaluation. Hence, the approach does not require explicit knowledge of $\underline{\Delta}^T$ and $\underline{\Delta}$. The underlying system property that is exploited here is linearity. A single iteration of the proposed Procedure 2 applied to a two-input two-output MIMO system is shown in Fig. 6.

C. Convergence and Implementation Aspects

1) Convergence Aspects: Procedures 1 and 2 are globally convergent. The proof follows directly from the power iterations method for computing the largest eigenvalue of a matrix, see [23, Sec. 8.2]. In addition, the finite time induced two norm in (12) converges to the $\mathcal{H}_\infty$ norm for $N \to \infty$, see [17, Th. 3]. Hence, N should be chosen sufficiently large to avoid transient effects. Such transient effects are well known in system identification, e.g., in frequency domain system identification these are directly related to leakage errors, see [24]. Also, note that this result differs from time-domain model

Authorized licensed use limited to: Zhejiang University. Downloaded on November 15,2024 at 14:52:51 UTC from IEEE Xplore. Restrictions apply.

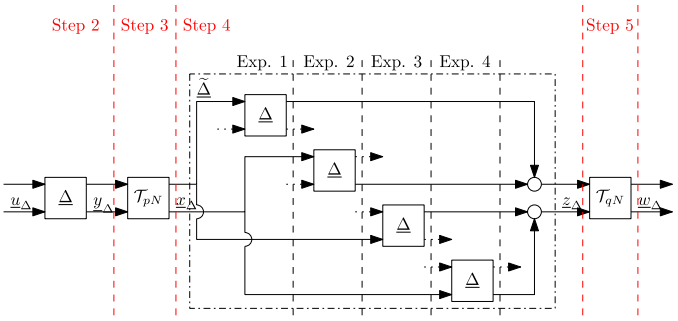

Fig. 6. Illustration of one iteration n of Procedure 2 for $p = q = 2$. The disconnected inputs are taken equal to zero. Different steps are indicated in red line. Step 4 involves four experiments that are explicitly indicated.

validation, including [13]. In particular, such model validation techniques also exploit the result (14) but are exact for both the infinite and finite time cases. The key difference lies in the fact that the power iteration approach in this paper involves an estimation problem instead of a model validation problem. The key advantage of the power iterations method is that very effectively deals with noise, as is described in Section III-C3. In fact, in [17, Sec. 4.2], it is shown that the power iterations method can be interpreted as an iterative experiment design approach for estimating the $\mathcal{H}_\infty$ norm.

2) Input Constraints: The actual implementation on physical systems of the data-driven $\mathcal{H}_\infty$ norm estimation Procedures 1 and 2 for SISO and MIMO systems, respectively, requires some additional attention. First, the input $\underline{u_\Delta}^{(n)}$ to the system Δ_o is usually subjected to constraints, including energy, power, and amplitude constraints. These constraints can directly be dealt with. In particular, let $\mu^{(n)}$ be a normalization constant such that the input

$$\frac{1}{\mu^{(n)}}\underline{u_\Delta}^{(n)} \tag{23}$$

satisfies the input constraints. Next, apply the scaled input in (23) to the system Δ_o. Then, by linearity

$$\mu^{(n)}\Delta_o\frac{1}{\mu^{(n)}}\underline{u_\Delta}^{(n)} = \Delta_o\underline{u_\Delta}^{(n)}.$$

Hence, either the output of Δ_o should be scaled by $\mu^{(n)}$ or the estimators $\hat{\gamma}_1$ and $\hat{\gamma}_2$ should be appropriately extended with the reciprocal of the normalization constant $\frac{1}{\mu^{(n)}}\mu^{(n)}$.

3) Noise Aspects: In Section III-A and III-B, an iterative estimation approach is presented that applies to the noise-free situation. A key aspect in any uncertainty modeling procedure for robust control involves the distinction between the exogenous noise and unmodeled dynamics. For instance, in model-validation approaches [10], [12], [13], it is tested whether there exists an element in the model uncertainty class and disturbance signal that explain the measured data. In contrast, the proposed power iteration method in Section III-A and III-B involve an estimation problem. In the case where additive noise affects the measurements, i.e., (13) is extended to $\underline{y_\Delta} = \underline{\Delta u_\Delta} + \underline{e}$, where e is zero-mean white noise with variance λ_e, then two aspects are relevant:

1) if $\underline{u_\Delta}$ is assumed to converge to the eigenvector corresponding to the largest eigenvalue $\lambda^{\max}(\mathcal{T}_N\underline{\Delta})$, see (16) for the SISO case, then the estimator (17) is unbiased and its variance decreases with N and is proportional to λ_e, see [16, Sec. 3.1] for a proof;
2) in [17], the convergence of the algorithm has been established in the situation where noise is present. In this case, the signal $\underline{u_\Delta}$ may not converge to the desired eigenvector. The noise affecting the output can be interpreted as a reinitialization of the algorithm. To avoid bias of the estimator $\hat{\gamma}_1^{(n)}$, it has been argued in [17] that the iterative procedure should be extended to ensure convergence.

Summarizing, the aspect of additive noise of the power iteration algorithm has been extensively addressed in [16, Sec. 3.1] and [17]. For the considered mechatronic application in this paper, the signal-to-noise ratio can be made sufficiently large by scaling the input appropriately using the results in Section III-C2. Thus, the input $\underline{u_\Delta}$ converges to the eigenvector corresponding to the largest eigenvalue and the estimators (17) and (22) are unbiased. In addition, due to a good signal-to-noise ratio and a relatively long experiment, the variance of the estimator is small.

IV. Toward a Multivariable Modeling Procedure for Achieving Robust Performance

In the previous section, a novel approach has been presented to estimate the $\mathcal{H}_\infty$ norm γ of the model error in (10). As is argued in Section II-D, two aspects are remaining that determine the shape of the model set $\mathcal{P}$, i.e.: 1) the nominal model $\hat{P}$ and 2) the uncertainty structure leading to $\hat{H}(\hat{P})$ in (9).

The shape of the model set $\mathcal{P}$ clearly determines the worst case performance bound in (6). In this section, a three-step procedure is proposed such that the nominal model $\hat{P}$, the uncertainty structure, i.e., $\hat{H}(\hat{P})$, and the approach in Section III-B to estimate γ jointly aim at achieving a small worst case performance bound in (6). This is of crucial importance in view of the approach in Section III-B that only delivers a norm-bound. In contrast, alternative uncertainty modeling procedures often adopt weighting functions to reduce conservatism, see [19, Sec. 7.4.3].

First, the general objective for modeling $\mathcal{P}$ is defined, after which the three steps are described in detail. These three steps constitute Contribution C2 of the paper and are summarized as follows.

Procedure 3: Perform the following three steps for identifying $\mathcal{P}$.

1) Identify $\hat{P}$ in (25), see Section IV-B.
2) Construct uncertainty model (27), leading to (28), see Section IV-C.
3) Apply Procedures 2 and 3, leading to γ and hence $\mathcal{P}$ in (9) and (10).

A. Modeling Goal

The function $\mathcal{J}_{\mathrm{WC}}(\mathcal{P}, C)$ is a complex function of both $\mathcal{P}$ and C. By noting that C^{RP} in (5) depends on $\mathcal{P}$, i.e.,

Authorized licensed use limited to: Zhejiang University. Downloaded on November 15,2024 at 14:52:51 UTC from IEEE Xplore. Restrictions apply.

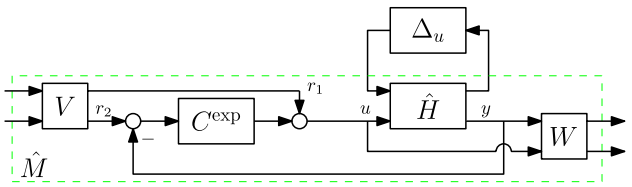

Fig. 7. Worst case performance $\mathcal{J}_{\rm WC}(\mathcal{P}, C^{\exp})$ cast into the generalized plant framework.

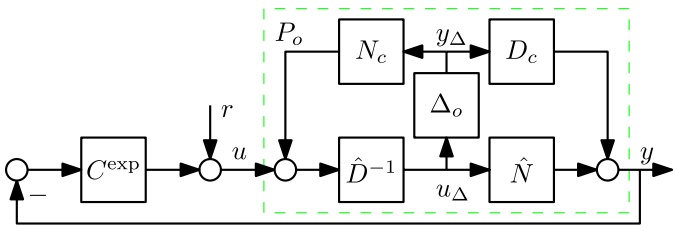

Fig. 8. Block diagram corresponding to uncertainty structure (27).

$C^{\rm RP}(\mathcal{P})$, it is desired to determine $\mathcal{P}$ such that it minimizes $\mathcal{J}_{\rm WC}(\mathcal{P}, C^{\rm RP}(\mathcal{P}))$, subjected to (4). However, this is in general difficult to solve.

The key step in this section is to exploit knowledge of $C^{\exp}$, see Section II-A, to obtain a tractable approach that is aimed at achieving high performance in (5). Note that, $\mathcal{J}_{\rm WC}(\mathcal{P}, C^{\rm RP}) \leq \mathcal{J}_{\rm WC}(\mathcal{P}, C^{\exp})$. Hence, $C^{\exp}$ provides an upper bound for the guaranteed performance in (5). Hence, the aim is to determine

$$\begin{aligned} \mathcal{P} = \ & \arg\min \mathcal{J}_{\rm WC}(\mathcal{P}, C^{\exp}) \\ & \text{subjected to } P_o \in \mathcal{P}. \end{aligned} \tag{24}$$

B. Step I: Nominal Modeling

In the first step, a nominal model $\hat{P}$ is identified. In view of (24), the control objective is also adopted in control-relevant identification. In particular, the control-relevant identification criterion in [25] is adopted, i.e., $\hat{P}$ is minimized according to

$$\min_{\hat{P}} \left\| WT(P_o, C^{\exp})V - WT(\hat{P}, C^{\exp})V \right\|_\infty. \tag{25}$$

The actual minimization in (25) is performed using the approach in [20] and is described in Section V-A. First, it is shown in Section IV-C that this criterion is useful in view of (24).

C. Step II: Uncertainty Model Structure Selection

Having identified a nominal model that minimizes (25), the next step is the selection of an uncertainty model structure that extends $\hat{P}$ to $\hat{H}(\hat{P})$. As in Step 1, the essence lies in selecting the uncertainty structure such that it facilitates solving (24).

To establish the connection between $\hat{H}(\hat{P})$ and the criterion (24), note that the latter can be expressed as an LFT. This involves the construction of a generalized plant, as explained in [19, Sec. 3.8]. In particular, the uncertain model $\mathcal{P}$ in (9) is appended with weighting filters and interconnected with $C^{\exp}$, leading to the setup in Fig. 7. Thus

$$\begin{aligned} & \mathcal{J}_{\rm WC}(\mathcal{P}, C^{\exp}) \\ & \quad = \sup_{\Delta_u \in \mathbf{\Delta}_u} \left\| \hat{M}_{22} + \hat{M}_{21}\Delta_u(I - \hat{M}_{11}\Delta_u)^{-1}\hat{M}_{12} \right\|_\infty. \end{aligned} \tag{26}$$

Since (26) depends on a complicated manner on Δ_u and hence γ, see (10), a specific approach that relies on the results in [20] is adopted. In particular, in [20], it is suggested to:

1) adopt the dual-Youla uncertainty structure [26], [27]

$$\mathcal{P}^{\rm DY} = \left\{ P \,|\, P = \left(\hat{N} + D_c\Delta_u\right)\left(\hat{D} - N_c\Delta_u\right)^{-1}, \Delta_u \in \mathbf{\Delta}_u \right\} \tag{27}$$

where;

2) the pair $\{\hat{N}, \hat{D}\}$ is a robust-control-relevant coprime factorization of $\hat{P}$, as defined in [20, Sec. 3.3];
3) the pair $\{N_c, D_c\}$ is a (W_u, W_y)-normalized coprime factorization of $C^{\exp}$, see [20, Def. 4].

In (27), $\{\hat{N}, \hat{D}\}$ is a coprime factorization of $\hat{P}$ if $\hat{P} = \hat{N}\hat{D}^{-1}$ and, in addition, $\hat{N}, \hat{D} \in \mathcal{RH}_\infty$ and $\exists X, Y$ such that $X\hat{N} + Y\hat{D} = I$. As a result of 1), 2), and 3), (26) simplifies to

$$\begin{aligned} \mathcal{J}_{\rm WC}(\mathcal{P}, C^{\exp}) & \leq \|\hat{M}_{22}\|_\infty + \sup_{\Delta_u \in \mathbf{\Delta}_u} \|\Delta_u\|_\infty \\ & = \mathcal{J}(\hat{P}, C^{\exp}) + \gamma \end{aligned} \tag{28}$$

see [20] for a proof of (28) and more details the specific coprime factorizations.

The result (28) provides a direct connection between the size γ of Δ_u, see (10), and the control criterion $\mathcal{J}_{\rm WC}(\mathcal{P}, C^{\exp})$. Interestingly, the size of model uncertainty γ in (28) is equal to the norm in the control-relevant identification objective (25). This implies that the same objective, i.e., (24), is being pursued during the nominal modeling step (Step I) and uncertainty modeling step (Step II).

D. Step III: Data-Driven Estimation of γ

Now, given $\hat{H}(\hat{P})$, it remains to estimate γ to complete the model set $\mathcal{P}$. In this step, γ is estimated using the multivariable data-driven $\mathcal{H}_\infty$ norm estimation Procedure 2.

The key observation from Section III is that Procedure 2 requires performing experiments on Δ_o, i.e., the specification of u_Δ and measurement of y_Δ. The first step in this section is to investigate how to gain access to u_Δ and y_Δ, given the uncertainty structure (27). As is described in Section III, the essential idea is to perform measurements on the Δ_o to determine its $\mathcal{H}_\infty$ norm γ. Note that, the Δ_o that induces P_o in (11) can be computed directly using (27), leading to

$$\Delta_o = D_c^{-1}(I + P_oC)^{-1}(P_o - \hat{P})\hat{D}. \tag{29}$$

The result (29) reveals that Δ_o depends on the model $\hat{P} = \hat{N}\hat{D}^{-1}$, the true system P_o, and $C^{\exp} = N_cD_c^{-1}$. Hence, it is expected that performing an experiment on Δ_o both involves computations using the model $\hat{P}$, as well as performing experiments with P_o.

To gain access to u_Δ and y_Δ, note that (27) in closed loop with $C^{\exp}$ implemented can be indicated, as in Fig. 8. Inspection reveals

$$u_\Delta = \hat{D}^{-1}(r - C^{\exp}\hat{N}u_\Delta - C^{\exp}D_cy_\Delta + N_cy_\Delta)$$

Authorized licensed use limited to: Zhejiang University. Downloaded on November 15,2024 at 14:52:51 UTC from IEEE Xplore. Restrictions apply.

implying that the reference signal

$$r = (\hat{D} + C^{\exp}\hat{N})u_\Delta \tag{30}$$

should be applied. Next, observe that

$$y_\Delta = D_c^{-1}(y - \hat{P}(I + C^{\exp}\hat{P})^{-1}r). \tag{31}$$

Equations (30) and (31) reveal how experiments can be performed on Δ_o. This is summarized in the following procedure.

Procedure 4 (Performing Experiments on Δ_o): Let input u_Δ be given and perform the following sequence of steps.

1) Compute $r = (\hat{D} + C^{\exp}\hat{N})u_\Delta$.
2) Perform a closed-loop experiment on P_o with $C^{\exp}$ implemented, i.e., $y = P_o(I + C^{\exp}P_o)^{-1}r$.
3) Compute $y_\Delta = D_c^{-1}(y - \hat{P}(I + C^{\exp}\hat{P})^{-1}r)$.

Procedure 4 can directly be implemented in Procedure 2, enabling the data-driven estimation for multivariable uncertainty structures given by (27).

Remark 1: Besides the fact that the specific coprime factor representation used in (27) leads to the result (28), the general representation of (27) has important consequences for the analysis of the algorithm in the presence of noise. Indeed, by the results presented in [28], the impact of noise that enters the feedback loop in fact is equivalent to an open-loop identification problem. Hence, the analysis of noise applied to open-loop systems in [17] directly applies to the closed-loop results presented in this paper.

V. Experimental Results Uncertainty Modeling

In this section, the multivariable modeling procedure presented in Section IV is applied to the AVIS in Section II-A. Together with Section VI, this constitutes Contribution C3 of this paper.

A. Step I. Nominal Modeling

In the first step, the nominal model $\hat{P}$ in (25) is identified. A frequency response function of the closed-loop system $T(P_o, C^{\exp})$ is identified using the approach in [24]. The key reason for the intermediate step of frequency response function identification is that it enables the solution of (25) by exploiting the frequency domain interpretation of the $\mathcal{H}_\infty$ norm. By exploiting a multisine experiment design, the approach in [24] enables the accurate identification of frequency response functions by effectively reducing the variance error without introducing bias. By virtue of (8), an estimate of P can be obtained from the relation $P = T_{12}T_{22}^{-1}$. The identified frequency response function of P_o is shown in Fig. 9.

Next, a model parameterization for $\hat{P}$ is used. An eighth-order model is used. The reason for this low order is that the criterion (25) essentially shapes the bias of the parametric model. Hence, a low-order model suffices for control purposes. The actual optimization is performed using the algorithm in [20, Sec. 3.4–3.5]. The resulting parametric model $\hat{P}$ is shown in Fig. 9. In addition, the nonparametric frequency response function of P_o is depicted. Inspection reveals that the suspended rigid-body mode at 4 Hz and the first resonance at 135 Hz are accurately modeled.

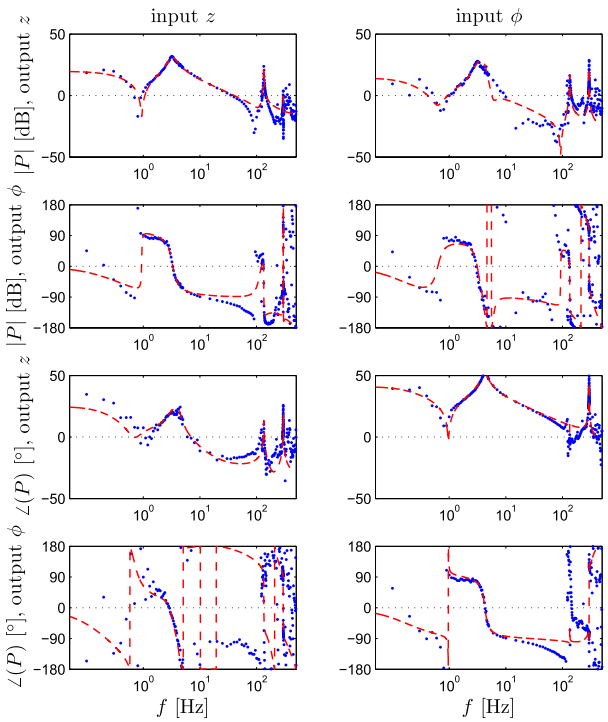

Fig. 9. Nonparametric frequency response function P_o (blue dots line) and identified parametric model $\hat{P}$ (dashed red line). Both the z-translation and ϕ-rotation are displayed.

B. Step II. Uncertainty Model Structure

Given the identified nominal model $\hat{P}$ in Step 1, the model uncertainty structure in (27) is constructed. Importantly, the required coprime factorizations in (27) follow directly from the pursued approach in [20], leading to the result (28).

To obtain an idea of the shape of Δ_o, the frequency response function of Δ_o is identified. To achieve this, Procedure 4 is employed in conjunction with the approach in [24, Ch. 2]. It is emphasized that the resulting frequency response function of Δ_o is not required for using the power iterations algorithm in Section III. However, it does provide insight into the shape of Δ_o and a reference value for γ. In particular, the peak value of $\bar{\sigma}(\Delta_u)$ over frequency equals 1.95, which is attained at a frequency of 296 Hz. Note that, a rather dense frequency grid has been employed to determine the frequency response function Δ_o, leading to a fairly long experimentation time.

In the following section, Procedure 2 is applied to estimate γ.

C. Step III. Data-Driven Estimation of γ

In this section, the key experimental results of this paper are presented, which involve the application of Procedure 2 in view of uncertainty modeling of the AVIS.

The application of Procedure 2 leads to the following observations.

1) The iteration is initialized with $\underline{u_\Delta}^{(1)}$ being zero mean white noise, see Figs. 11 (Iteration 1) and 12 (Iteration 1) for the corresponding power spectral density $\Psi_{\underline{u_\Delta}^{(1)}}$.

Authorized licensed use limited to: Zhejiang University. Downloaded on November 15,2024 at 14:52:51 UTC from IEEE Xplore. Restrictions apply.

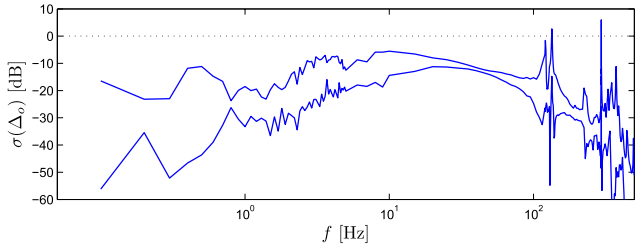

Fig. 10. Frequency response function estimate of Δ_o.

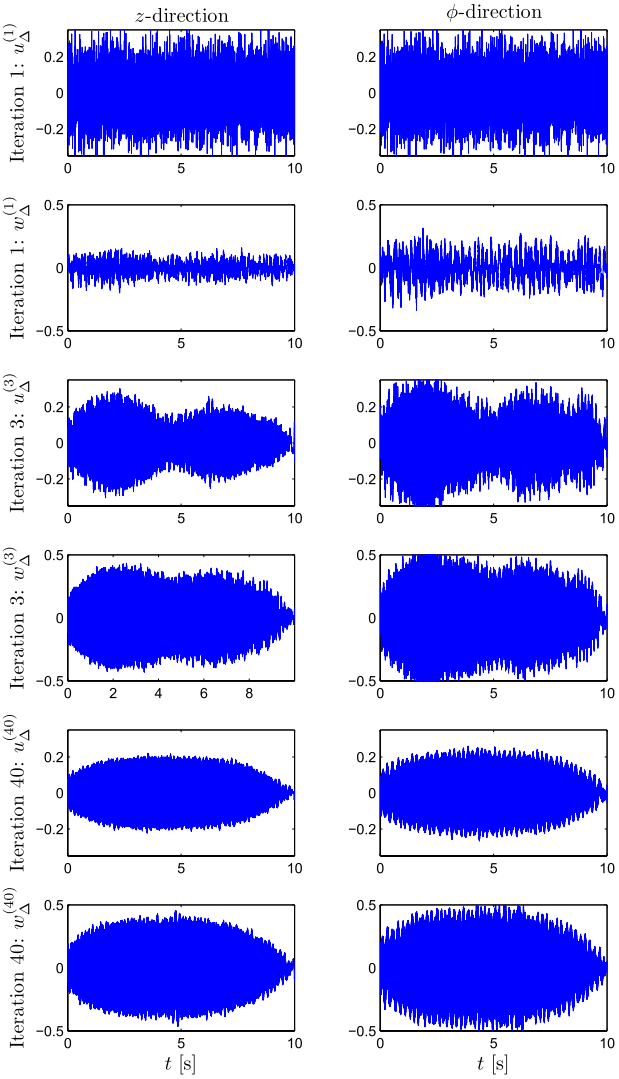

Fig. 11. Power iterations: iterations 1 (top), 3 (middle), and 40 (bottom) of Procedure 2–measured inputs $\underline{u}_\Delta$ and outputs $\underline{w}_\Delta$.

2) The output $\underline{w}_\Delta{}^{(1)}$ of $\Delta_o^T\Delta_o$ in Fig. 11 (Iteration 1) is colored noise, since it contains several dominant frequency components.
3) The resulting input $\underline{u}_\Delta$ and output $\underline{w}_\Delta$ in iteration $n = 3$ are shown in Figs. 11 (Iteration 3) and 12 (Iteration 3). Both $\underline{u}_\Delta$ and $\underline{w}_\Delta$ contain several dominant frequency components. In addition, note that the inputs during the different iterations are normalized with respect to the two norm. Interestingly, the output in iteration $n = 3$ already has a significantly larger amplitude compared with the output in iteration $n = 1$, see Fig. 11.
4) After 40 iterations, the input is mostly sinusoidal except for truncation effects, see Figs. 11 and 12.
5) After convergence, $\underline{u}_\Delta{}^{(40)}$ is nonzero in both z- and ϕ-direction, see Figs. 11 and 12. Hence, Procedure 2 also determines the worst case input direction.

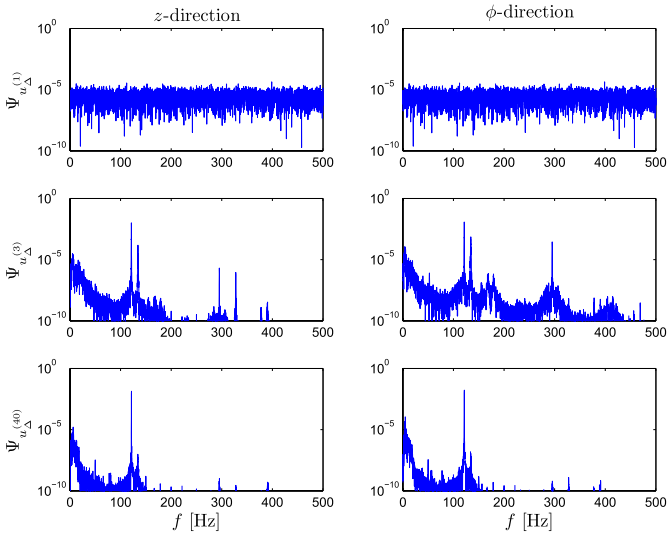

Fig. 12. Power iterations: iterations 1 (top), 3 (middle), and 40 (bottom) of Procedure 2–power spectral density of the input $\underline{u}_\Delta$.

Next, estimator (22) is evaluated for all 40 iterations, see Fig. 13. This leads to the following observations. First, the estimate $\hat{\gamma}_2^{(n)}$ converges for increasing n. This leads to

$$\hat{\gamma}_2^{(40)} = 1.997.$$

Second, when comparing the estimated $\hat{\gamma}_2^{(40)} = 1.997$ with the result in Section V-B, which is based on the frequency response function estimate in Fig. 10, it is observed that Procedure 2 leads to a higher value $\hat{\gamma}_2^{(40)}$ compared to $\sup_\omega \bar{\sigma}(\Delta_o)$. Interestingly, inspection of Fig. 12 (Iteration 40) reveals that the dominant frequency component is 121 Hz, which differs significantly from the worst case frequency of 296 Hz that was obtained in Section V-B. Hence, due to its guaranteed global convergence, Procedure 2 provides an effective means for determining the worst case frequency in view of $\mathcal{H}_\infty$ norm estimation. This is in sharp contrast to the situation where a fixed prechosen frequency grid is used, as is confirmed by the considered application. In this respect, Procedure 2 is considered as a useful adaptive experiment design approach.

D. Summary

The obtained nominal model $\hat{P}$ in Step I, together with the uncertainty structure in Step II, and the size $\hat{\gamma}_2^{(40)} = 1.997$ in Step III, lead to a model set $\mathcal{P}$, see (9). In the following section, the model set $\mathcal{P}$ is used to design a robust controller.

VI. Controller Synthesis and Experimental Implementation

A. Robust Controller Synthesis

The model set $\mathcal{P}$ is used to analyze and synthesize several controllers. In particular, the following controllers are

Authorized licensed use limited to: Zhejiang University. Downloaded on November 15,2024 at 14:52:51 UTC from IEEE Xplore. Restrictions apply.

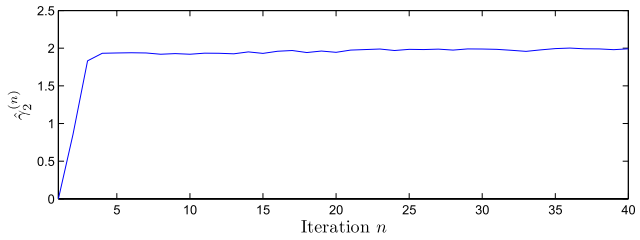

Fig. 13. Estimated norm $\hat{\gamma}_2^{(n)}$.

TABLE I
ROBUST-CONTROL-RELEVANT IDENTIFICATION AND ROBUST CONTROLLER SYNTHESIS RESULTS

Controller	Minimized criterion	$\mathcal{J}(\hat{P}, C)$	$\mathcal{J}_{\mathrm{WC}}(\mathcal{P}, C)$
C^{exp}	None	14.30	16.30
C^{NP}	$\mathcal{J}(\hat{P}, C)$	1.87	∞
C^{RP}	$\mathcal{J}_{\mathrm{WC}}(\mathcal{P}, C)$	4.80	5.02

considered:

C^{exp}: initial controller that is described in Section II-A;
C^{NP}: nominal controller $C^{\mathrm{NP}} = \arg\min_C \mathcal{J}(\hat{P}, C)$;
C^{RP}: robust controller for model set $\mathcal{P}$ in (5).

The controllers C^{NP} and C^{RP} are computed using $\mathcal{H}_\infty$-optimization and skewed-μ-synthesis, see [19] for details.

The controllers are shown in Fig. 14, whereas the closed-loop process sensitivity functions $\hat{P}(I + C\hat{P})^{-1}$ are shown in Fig. 15. In addition, the achieved performance for both the model $\hat{P}$ and the model set $\mathcal{P}$ in terms of the control criterion are shown in Table I.

The following observations are made.

1) When comparing $\mathcal{J}(\hat{P}, C^{\mathrm{exp}})$ and $\mathcal{J}_{\mathrm{WC}}(\mathcal{P}, C^{\mathrm{exp}})$, it is observed that the bound (28) indeed holds and is tight.
2) From Table I, C^{NP} indeed achieves optimal performance for the nominal model $\hat{P}$. However, $\mathcal{J}_{\mathrm{WC}}(\mathcal{P}, C^{\mathrm{NP}})$ is unbounded. Hence, performance and stability cannot be guaranteed when implementing C^{NP} on P_o.
3) The controller C^{RP} achieves the smallest worst case performance, i.e., $\mathcal{J}_{\mathrm{WC}}(\mathcal{P}, C^{\mathrm{RP}})$. In addition, the performance for the nominal model, i.e., $\mathcal{J}(\hat{P}, C^{\mathrm{RP}})$ is also significantly improved when compared with $\mathcal{J}(\hat{P}, C^{\mathrm{exp}})$.
4) The improved performance in terms of the criterion coincides with improved disturbance attenuation properties at low frequencies in Fig. 15, see also Section II-A.

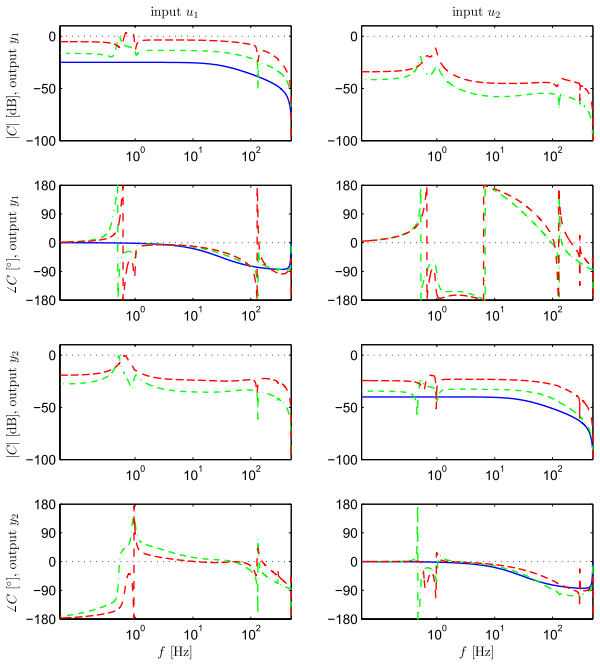

Fig. 14. Controllers: C^{exp} (solid blue line), C^{NP} (dashed red line), and C^{RP} (dashed-dotted green line).

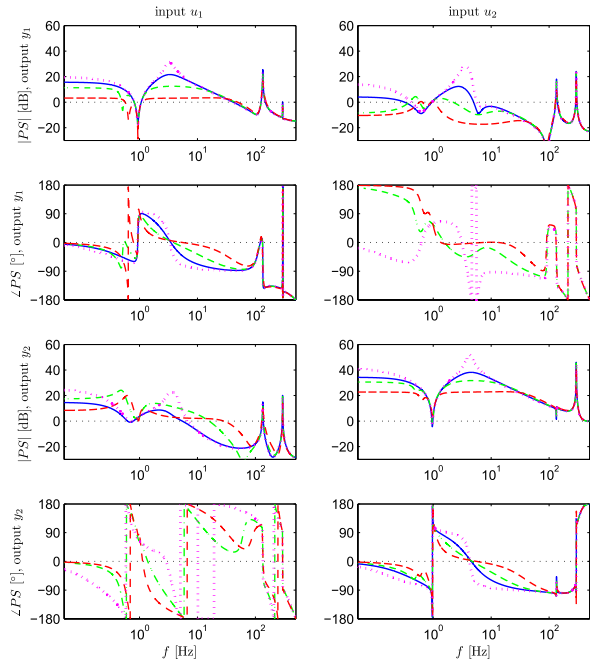

Fig. 15. Closed-loop process sensitivities: $\hat{P}(I + C^{\mathrm{exp}}\hat{P})^{-1}$ (solid blue line), $\hat{P}(I + C^{\mathrm{NP}}\hat{P})^{-1}$ (dashed red line), and $\hat{P}(I + C^{\mathrm{RP}}\hat{P})^{-1}$ (dashed-dotted green line). In addition, the nominal model $\hat{P}$ is depicted (dotted magenta line).

B. Controller Implementation

The synthesized controllers in Section VI-A are now implemented for validation. Measured time domain responses are shown in Fig. 16, whereas the corresponding cumulative power spectral (CPS) densities are shown in Fig. 17.

The following observations are made. First, the controller C^{NP} does not stabilize the actual system. This is observed from the response in the ϕ-direction in Fig. 16, where the system hits a safety guardrail due to the unstable behavior. This corroborates the results in Table I, where $\mathcal{J}_{\mathrm{WC}}(\mathcal{P}, C^{\mathrm{NP}})$ is unbounded, and hence no performance and stability guarantees can be given when implementing C^{NP} on the true system P_o.

Second, the experimental controller C^{exp} and optimal robust controller C^{RP} both stabilize the true system, which is revealed by the stationary behavior in Fig. 16. In addition, the controller C^{RP} leads to a significantly better performance when compared with C^{exp}, which is visible from the time-domain

Authorized licensed use limited to: Zhejiang University. Downloaded on November 15,2024 at 14:52:51 UTC from IEEE Xplore. Restrictions apply.

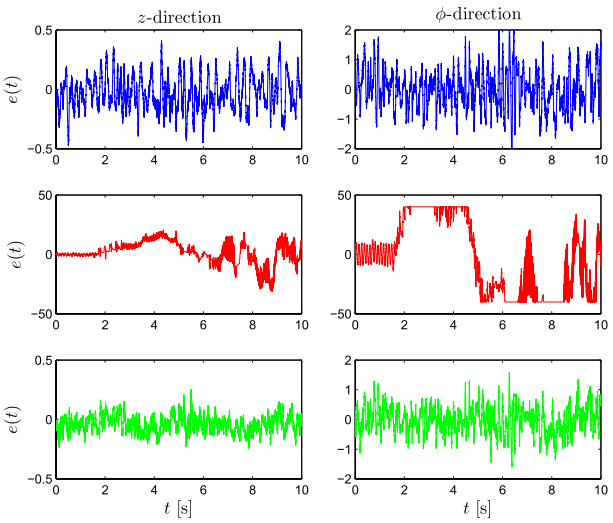

Fig. 16. Measured time-domain responses: C^{exp} (solid blue line, top), C^{NP} (dashed red line, middle), and C^{RP} (dashed-dotted green line, bottom). Here, low-frequency noise (normally distributed white noise, filtered through a low-pass filter with cutoff frequency of 8 Hz) is added to the system in both the z-translation and ϕ-rotation simultaneously.

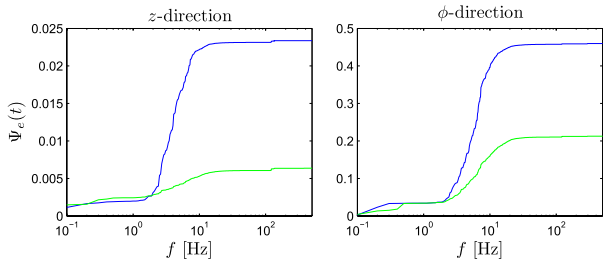

Fig. 17. CPS density of the measured error signals in Fig. 16: C^{exp} (solid blue line, top), C^{RP} (dashed-dotted green line, bottom).

responses in Fig. 16 and especially from the CPS density in Fig. 17. In particular, the controller C^{RP} leads to a performance improvement of more than a factor 4 in z-translation and more than a factor 2 in ϕ-rotation.

VII. Discussion

1) Model-Error Modeling Perspective: From the perspective of model-error modeling, the proposed approach does not require severe prior assumptions as in alternative approaches. Hence, it provides stronger guarantees in robust control design.

As is experimentally shown in Section V, Procedure 2 leads to a higher and hence more accurate estimation of the $\mathcal{H}_\infty$ norm compared with the use of an *a priori* chosen frequency grid, as is exemplified in Section V-B and also done in, see [8]. From this perspective, Procedure 2 can be observed as an adaptive experiment design procedure. Thus, Procedure 2 reduces estimation errors due to the use of a discrete frequency grid when compared with the uncertainty modeling procedure in [8]. From this perspective, it is emphasized that the use of prior assumptions to bound the interpolation error, as is done in, see [9] and [10], is likely to lead to conservative results, as is also argued in [11, 9.5.2].

2) Connections to Related (Iterative) Approaches: The approach presented in Section III is related to several identification and iterative control algorithms. For a connection to maximum-likelihood estimation, see [17, Remark 10].

The iterative algorithm in Section III can be related to iterative learning control (ILC) algorithms [29]. For simplicity, consider the situation of Procedure 1, in which case the input during the next iteration is given by

$$\underline{u_\Delta}^{(n+1)} = \mathcal{T}_N \underline{w_\Delta}^{(n)}$$

which closely resembles ILC update laws that are typically also a linear function of the signals $\underline{w_\Delta}^{(n)}$ and $\underline{u_\Delta}^{(n)}$. However, there are some principal differences when comparing typical ILC algorithms and Procedure 1. To show this, assume as in Section III-C that an input normalization is implemented[1] as in (23), with $\mu^{(n+1)} = \|\underline{w_\Delta}^{(n)}\|_2$, i.e., the two norm of the input is normalized to 1, as is also done in [17]. This leads to the input of the true system

$$\overline{\underline{u_\Delta}}^{(n+1)} = \frac{1}{\|\underline{w_\Delta}^{(n)}\|_2}\underline{u_\Delta}^{(n+1)} = \frac{1}{\|\underline{w_\Delta}^{(n)}\|_2}\mathcal{T}_N \underline{w_\Delta}^{(n)}$$

with output

$$\underline{w_\Delta}^{(n+1)} = \Delta_o \overline{\underline{u_\Delta}}^{(n+1)} = \Delta_o \frac{1}{\|\underline{w_\Delta}^{(n)}\|_2}\mathcal{T}_N \underline{w_\Delta}^{(n)}. \quad (32)$$

In (32), the operator $\Delta_o \frac{1}{\|\underline{w_\Delta}^{(n)}\|_2}\mathcal{T}_N$ maps $\mathbb{R}^N$ onto itself. Note that, the amplification of Δ_o for the input $\underline{w_\Delta}^{(n)}$ equals the two norm of the output $\underline{w_\Delta}^{(n+1)}$. Under mild assumptions, which are related to the comment in [17, Remark 9], $\|\underline{w_\Delta}^{(n+1)}\|_2 > \|\underline{w_\Delta}^{(n)}\|_2$. Since $\mathcal{T}$ has induced two norm equal to one, the induced two norm of $\Delta_o \frac{1}{\|\underline{w_\Delta}^{(n)}\|_2}\mathcal{T}_N$ is larger than one. Thus, (32) is a Lipschitz continuous function with Lipschitz constant larger than one, hence (32) is not a contraction. In contrast, ILC algorithms are also of the form (32), but designed such that the iteration (32) is a contraction map, corresponding to a Lipschitz constant that is strictly smaller than one. This ensures convergence to a unique fixed point, generally being an error signal of the system converging to zero.

The novel multivariable result of Procedure 2 provides further extensions to the implementation of ILC algorithms. In particular, in certain ILC algorithms referred to as adjoint ILC algorithms [30], it is desired to filter through the transpose of the system. It is clear that the use of time reversal operators as in (15) enables a direct evaluation on the true system and effectively renders the need for a model in ILC algorithms superfluous. Interestingly, a slight modification of Procedure 2 directly enables its use for multivariable ILC algorithms.

VIII. Conclusion

In this paper, a novel data-driven $\mathcal{H}_\infty$ norm estimation procedure, which relies on iterative experiments on the system, is proposed for multivariable systems. This procedure is employed for model-error modeling purposes, and embedded in a system identification and robust control design framework. The key advantage of the proposed approach is that it provides guarantees to satisfy (4) without relying on severe

[1] As is argued in Section III-C, this requires a slight modification of the estimators (17) and (22), see also [17].

Authorized licensed use limited to: Zhejiang University. Downloaded on November 15,2024 at 14:52:51 UTC from IEEE Xplore. Restrictions apply.

prior assumptions that are adopted in alternative approaches. Experimental results of an AVIS show fast convergence of the algorithm and its ability to determine both the worst case frequency and worst case input and output directions in $\mathcal{H}_\infty$ norm estimation. In addition, the experimental results confirm its ability to provide enhanced vibration isolation properties through a robust control design. Finally, the experimental results confirm that the iterative algorithm is useful for experiment design, i.e., to iteratively/adaptively determine improved inputs for $\mathcal{H}_\infty$ norm estimation, leading to improved results compared with existing approaches.

The proposed results can be directly extended. In addition to its possible use in ILC algorithms, see Section VII-2, it can be directly used in any multivariable estimation problem involving eigenvalues. In addition, the proposed approach exhibits global convergence for multivariable systems (see Section III-C). This requires an additional number of experiments, as is shown in Fig. 6. Present research focuses on reducing the number of experiments.

ACKNOWLEDGMENT

The authors would like to thank O. Bosgra, R. van Herpen, and B. Wahlberg for their contribution to this paper.

REFERENCES

[1] C. R. Fuller, S. J. Elliott, and P. A. Nelson, *Active Control of Vibration*. San Diego, CA, USA: Academic, 1996.

[2] A. Preumont, *Vibration Control of Active Structures: An Introduction* (Solid Mechanics and Its Applications), vol. 96, 2nd ed. New York, NY, USA: Kluwer, 2004.

[3] D. Karnopp, "Active and semi-active vibration isolation," *J. Mech. Des.*, vol. 117, pp. 177–185, Jun. 1995.

[4] Y. Zhang, A. G. Alleyne, and D. Zheng, "A hybrid control strategy for active vibration isolation with electrohydraulic actuators," *Control Eng. Pract.*, vol. 13, no. 3, pp. 279–289, Mar. 2005.

[5] Y. Chida, Y. Ishihara, T. Okina, T. Nishimura, K. Ohtomi, and R. Furukawa, "Identification and frequency shaping control of a vibration isolation system," *Control Eng. Pract.*, vol. 16, no. 6, pp. 711–723, Jun. 2008.

[6] W. Reinelt, A. Garulli, and L. Ljung, "Comparing different approaches to model error modeling in robust identification," *Automatica*, vol. 38, no. 5, pp. 787–803, May 2002.

[7] L. Ljung, "Model validation and model error modeling," in *Proc. Åström Symp. Control*, 1999, pp. 15–42.

[8] M. van de Wal, G. van Baars, F. Sperling, and O. Bosgra, "Multivariable $\mathcal{H}_\infty/\mu$ feedback control design for high-precision wafer stage motion," *Control Eng. Pract.*, vol. 10, no. 7, pp. 739–755, Jul. 2002.

[9] D. K. de Vries and P. M. J. Van den Hof, "Quantification of model uncertainty from data," *Int. J. Robust Nonlinear Control*, vol. 4, no. 2, pp. 301–319, 1994.

[10] J. Chen and G. Gu, *Control-Oriented System Identification: An $\mathcal{H}_\infty$ Approach*. New York, NY, USA: Wiley, 2000.

[11] G. Vinnicombe, *Uncertainty and Feedback: $\mathcal{H}_\infty$ Loop-Shaping and the ν-Gap Metric*. London, U.K.: Imperial College Press, 2001.

[12] R. S. Smith and J. C. Doyle, "Model validation: A connection between robust control and identification," *IEEE Trans. Autom. Control*, vol. 37, no. 7, pp. 942–952, Jul. 1992.

[13] K. Poolla, P. Khargonekar, A. Tikku, J. Krause, and K. Nagpal, "A time-domain approach to model validation," *IEEE Trans. Autom. Control*, vol. 39, no. 5, pp. 951–959, May 1994.

[14] T. Oomen and O. Bosgra, "Well-posed model uncertainty estimation by design of validation experiments," in *Proc. 15th IFAC Symp. Syst. Identificat.*, Saint-Malo, France, Jul. 2009, pp. 1199–1204.

[15] H. Hjalmarsson, "From experiment design to closed-loop control," *Automatica*, vol. 41, pp. 393–438, Jan. 2005.

[16] B. Wahlberg, M. Barenthin Syberg, and H. Hjalmarsson, "Non-parametric methods for $\mathcal{L}_2$-gain estimation using iterative experiments," *Automatica*, vol. 46, no. 8, pp. 1376–1381, 2010.

[17] C. R. Rojas, T. Oomen, H. Hjalmarsson, and B. Wahlberg, "Analyzing iterations in identification with application to nonparametric $\mathcal{H}_\infty$-norm estimation," *Automatica*, vol. 48, no. 11, pp. 2776–2790, 2012.

[18] M. Barenthin, M. Enqvist, B. Wahlberg, and H. Hjalmarsson, "Gain estimation for Hammerstein systems," in *Proc. 14th IFAC Symp. Syst. Identificat.*, Newcastle, Australia, Mar. 2006, pp. 784–789.

[19] S. Skogestad and I. Postlethwaite, *Multivariable Feedback Control: Analysis and Design*, 2nd ed. West Sussex, U.K.: Wiley, 2005.

[20] T. Oomen and O. Bosgra, "System identification for achieving robust performance," *Automatica*, vol. 48, no. 9, pp. 1975–1987, Sep. 2012.

[21] T. Oomen, R. van der Maas, C. R. Rojas, and H. Hjalmarsson, "Iteratively learning the $\mathcal{H}_\infty$-norm of multivariable systems applied to model-error-modeling of a vibration isolation system," in *Proc. ACC*, Washington, DC, USA, Jun. 2013, pp. 6718–6723.

[22] D. C. McFarlane and K. Glover, *Robust Controller Design Using Normalized Coprime Factor Plant Descriptions* (Lecture Notes in Control and Information Sciences), vol. 138. Berlin, Germany: Springer-Verlag, 1990.

[23] G. H. Golub and C. F. Van Loan, *Matrix Computations*, 3rd ed. Baltimore, MD, USA: The Johns Hopkins Univ. Press, 1996.

[24] R. Pintelon and J. Schoukens, *System Identification: A Frequency Domain Approach*, 2nd ed. New York, NY, USA: IEEE Press, 2012.

[25] R. J. P. Schrama, "Accurate identification for control: The necessity of an iterative scheme," *IEEE Trans. Autom. Control*, vol. 37, no. 7, pp. 991–994, Jul. 1992.

[26] S. G. Douma and P. M. J. Van den Hof, "Relations between uncertainty structures in identification for robust control," *Automatica*, vol. 41, no. 3, pp. 439–457, Mar. 2005.

[27] R. A. de Callafon and P. M. J. Van den Hof, "Suboptimal feedback control by a scheme of iterative identification and control design," *Math. Model. Syst.*, vol. 3, no. 1, pp. 77–101, 1997.

[28] F. Hansen, G. Franklin, and R. Kosut, "Closed-loop identification via the fractional representation: Experiment design," in *Proc. ACC*, Pittsburgh, PA, USA, Jun. 1989, pp. 1422–1427.

[29] D. A. Bristow, M. Tharayil, and A. G. Alleyne, "A survey of iterative learning control: A learning-based method for high-performance tracking control," *IEEE Control Syst.*, vol. 26, no. 3, pp. 96–114, Jun. 2006.

[30] J. D. Ratcliffe, J. J. Hätönen, P. L. Lewin, E. Rogers, and D. H. Owens, "Robustness analysis of an adjoint optimal iterative learning controller with experimental verification," *Int. J. Robust Nonlinear Control*, vol. 18, no. 10, pp. 1089–1113, Jul. 2008.

Tom Oomen (M'06) received the M.Sc. (*cum laude*) and Ph.D. degrees from the Eindhoven University of Technology, Eindhoven, The Netherlands, in 2005 and 2010, respectively.

He is currently an Assistant Professor with the Department of Mechanical Engineering, Eindhoven University of Technology. He held visiting positions with the KTH Royal Institute of Technology, Stockholm, Sweden, and the University of Newcastle, Callaghan, Australia. His current research interests include system identification and robust control with applications in high-precision mechanical servo systems.

Dr. Oomen was a recipient of the Corus Young Talent Graduation Award in 2005. He is an Associate Editor with the IEEE Conference Editorial Board and a Guest Editor for IFAC Mechatronics.

Rick van der Maas (M'13) received the M.Sc. degree in mechanical engineering from the Eindhoven University of Technology, Eindhoven, The Netherlands, in 2011, where he is currently pursuing the Ph.D. degree in mechanical engineering.

His current research interests include system identification, modeling, and control with applications in high-precision and medical imaging systems.

Authorized licensed use limited to: Zhejiang University. Downloaded on November 15,2024 at 14:52:51 UTC from IEEE Xplore. Restrictions apply.

Cristian R. Rojas (M'13) was born in 1980. He received the M.S. degree in electronics engineering from Universidad Técnica Federico Santa María, Valparaíso, Chile, and the Ph.D. degree in electrical engineering from the University of Newcastle, Callaghan, Australia, in 2004 and 2008, respectively.

He has been with the Royal Institute of Technology, Stockholm, Sweden, since 2008, where he is currently an Assistant Professor with the Automatic Control Laboratory, School of Electrical Engineering. His current research interests include system identification and signal processing.

Håkan Hjalmarsson (M'98–SM'11–F'13) was born in 1962. He received the M.S. degree in electrical engineering, and the Licentiate and Ph.D. degrees in automatic control from Linköping University, Linköping, Sweden, in 1988, 1990, and 1993, respectively.

He held visiting research positions with the California Institute of Technology, Pasadena, CA, USA, Louvain University, Louvain-La-Neuve, Belgium, and the University of Newcastle, Callaghan, Australia. He is a Professor with the School of Electrical Engineering, KTH Royal Institute of Technology, Stockholm, Sweden. His current research interests include system identification, signal processing, control and estimation in communication networks, and automated tuning of controllers.

Dr. Hjalmarsson has served as an Associate Editor for *Automatica* from 1996 to 2001 and the IEEE TRANSACTIONS ON AUTOMATIC CONTROL from 2005 to 2007, and a Guest Editor for the *European Journal of Control and Control Engineering Practice*. He is a Chair of the IFAC Coordinating Committee CC1 Systems and Signals. In 2001, he received the KTH Award for outstanding contribution to undergraduate education. He is a co-recipient of the European Research Council Advanced Grant.

Authorized licensed use limited to: Zhejiang University. Downloaded on November 15,2024 at 14:52:51 UTC from IEEE Xplore. Restrictions apply.